AD_____

Award Number: W81XWH-11-1-0371

TITLE: Intracellular Protein Delivery for treating Breast Cancer

PRINCIPAL INVESTIGATOR: Yi Tang

CONTRACTING ORGANIZATION: University of California Los Angeles
Los Angeles, CA 90095

REPORT DATE: June 2013

TYPE OF REPORT: Annual

PREPARED FOR: U.S. Army Medical Research and Materiel Command
Fort Detrick, Maryland 21702-5012

REPORT DOCUMENTATION PAGE

Form Approved
OMB No. 0704-0188

1. REPORT DATE	2. REPORT TYPE	3. DATES COVERED
June 2013	Annual	15 May 2012 to 14 May 2013

4. TITLE AND SUBTITLE
Intracellular Protein Delivery for treating Breast Cancer

5a. CONTRACT NUMBER

5b. GRANT NUMBER
W81XWH-11-1-0371

5c. PROGRAM ELEMENT NUMBER

6. AUTHOR(S)
Yi Tang

E-Mail: yitang@ucla.edu

5d. PROJECT NUMBER

5e. TASK NUMBER

5f. WORK UNIT NUMBER

7. PERFORMING ORGANIZATION NAME(S) AND ADDRESS(ES)
University of California Los Angeles

Los Angeles, CA 90095

8. PERFORMING ORGANIZATION REPORT NUMBER

9. SPONSORING / MONITORING AGENCY NAME(S) AND ADDRESS(ES)
U.S. Army Medical Research and Materiel Command
Fort Detrick, Maryland 21702-5012

10. SPONSOR/MONITOR'S ACRONYM(S)

11. SPONSOR/MONITOR'S REPORT NUMBER(S)

12. DISTRIBUTION / AVAILABILITY STATEMENT
Approved for Public Release; Distribution Unlimited

13. SUPPLEMENTARY NOTES

14. ABSTRACT

Specific induction of cell death in tumors is considered one of the most desired and effective anticancer therapies. Effective strategies to activate the apoptotic pathway, or other death mechanisms, are currently being intensely pursued. A potent chemotherapy option is directly arming the cancer cells with executioner proteins or apoptotic-inducing proteins that are not targeted by anti-apoptotic maneuvers found in many tumors. During this period, we showed that the tumor suppressor, cellular guardian p53 can be recombinantly produced, encapsulated into polymeric nanocapsules, and be delivered to different cancer cell lines. The super p53, which contains the S121F mutation can selectively kill tumor cells. In addition, we also developed a new nanocapsule synthesis strategy that allowed facile modification of polymer surface with tumor targeting ligands using click chemistry. Using such modified nanocapsule, we demonstrate the p53 cargo is only internalized into cancer cells that overexpress the targeting receptor. Animal studies will be performed in the next period (no cost extension).

15. SUBJECT TERMS
Nanogels, core-shell, redox-responsive, apoptosis, breast cancer.

16. SECURITY CLASSIFICATION OF:			17. LIMITATION OF ABSTRACT	18. NUMBER OF PAGES	19a. NAME OF RESPONSIBLE PERSON
					USAMRMC
a. REPORT	b. ABSTRACT	c. THIS PAGE			19b. TELEPHONE NUMBER *(include area code)*
U	U	U	UU	22	(310)825-0375

Table of Contents

INTRODUCTION

Specific induction of cell death in tumors is considered one of the most desired and effective anticancer therapies. Effective strategies to activate the apoptotic pathway, or other death mechanisms, are currently being intensely pursued. A potent chemotherapy option is directly arming the cancer cells with executioner proteins or apoptotic-inducing proteins that are not targeted by anti-apoptotic maneuvers found in many tumors. In this proposal, we will develop a new method to treat breast cancer by using a native-protein delivery approach. This is a platform to deliver proteins in native forms into cells. The key design feature of our strategy is to first encapsulate protein molecules in a thin layer of water soluble, positively charged, degradable polymer to form nanometer-sized nanocapsules. The nanocapsule shell facilitates uptake of the protein content into cells, and protects the protein both during in vivo circulation and endocytosis. To endow the nanocapsules biodegradability once entered the target cells, the polymer shell is crosslinked with redox-sensitive crosslinkers that can be reduced upon encountering the reducing environment of the cytoplasm. Our overall research objective is to thoroughly evaluate this delivery method as a potentially new therapeutic modality for breast cancer treatment. Three aims will be pursued in parallel and results from each aim will be used to guide the refinement of other aims and the overall research objective. 1) Delivering different target proteins to breast cancer cell lines using this approach, including the tumor specific apoptin; 2) Equipping the protein nanocapsules with specific cancer cell targeting ligands; 3) Examining the in vivo potency and pharmacokinetics of the nanocapsules.

BODY

Summary of State of Work

Specific Aim 1: Delivering different target proteins to breast cancer cell lines using protein nanocapsules

Task 1. Preparing and characterizing of Apoptin contained nanocapsules

This task has been completed and published in *Nano Today,* **2013, 8,** 11-20.

We are also characterizing a new nanocapsule formulation in which the transcription factor P53 is included.

Task 2. *in vitro* studying Apoptin contained nanocapsules

This task has been completed and published in *Nano Today,* **2013, 8,** 11-20.

We are also characterizing a new nanocapsule formulation in which the transcription factor P53 is included.

Specific Aim 2: Equipping protein nanocapsules with specific cancer cell targeting ligands;

Task 3. Preparing and testing of MMP activatable cell penetrating peptides (ACCPs)-coupled nanocapsules

Task 4. Preparing and testing of ligand-receptor affinity based targeting: Transferrin (Tf) and Herceptin

To accomplish this we are using a new conjugation approach and will be described.

Specific Aim 3: Examining the *in vivo* potency and pharmacokinetics of the nanocapsules.

Task 5. Evaluating *in vivo* distribution of protein nanocapsules

This task has been partially performed and some results will be in the following pages.

Task 6. Examining the *in vivo* pharmacokinetics of nanocapsules

This task is currently under evaluation, no results to report at this point.

Task 7. Determing the *in vivo* delivery efficacy of nanocapsules

This task has been completed and published in *Nano Today,* **2013, 8,** 11-20.

Additional in vivo experiment has been planned in collaboration with the Institute of Myeloma and Bone Cancer Research Institute and will be performed during the No Cost Extension period.

The work on apoptin nanocapsule described in the previous annual report (2011-2012) was recently published in Zhao et al, *Nano Today,* **2013, 8,** 11-20. **The Manuscript is included in the appendix.**

1. BACKGROUND AND MOTIVATION

The most desirable cancer therapy is both potent and specific towards tumor cells. Many conventional small molecule chemotheraputics do not discriminate between cancerous and normal cells, cause undesirable damage to healthy tissues, and are therefore unable to be administered at high dosage. In contrast, cytoplasmic and nuclear proteins that selectively alter the signaling pathways in tumor cells, reactivate apoptosis and restore tissue homeostasis, can eliminate cancerous cells and delay tumor progression with less collateral damage to other tissues. Using stimuli-responsive nanoscaled carriers for the intracellular delivery of such proteins, including human tumor suppressors (such as p53) and exogenous tumor-killing proteins (such as apoptin), is attractive as a new anti-cancer therapy modality.

Virtually all human cancer cells, including breast carcinomas, have elaborate anti-apoptotic strategies to overcome apoptosis, which is a vital cellular mechanism to obstruct tumor progression (Cotter, 2009). The most commonly mutated gene in tumor cells is the tumor suppressor gene *TP53*, the protein product of which promotes apoptosis of aberrant cells through both transcription-dependent and independent mechanisms (Coles et al., 1992). In this manner, p53 is critically important in eliminating possible neoplastic cells incurred during DNA damage. p53 has also recently been shown to be involved in restricting the metabolic flux through the pentose-phosphate pathway, which is needed for nutrient support during tumor proliferation (Wu et al., 2011). About 50% of all the human tumors have mutant p53 proteins, whereas ~30% of breast cancer cell lines are mutated in p53 (Lacroix et al., 2006). Breast tumors expressing mutant p53 are more frequently ER- and PR-, and are associated with a high proliferation rate, high histological and nuclear grades, aneuploidy, and poorer survival (Lacroix et al., 2006). Mutations of p53 confer a worse overall and disease-free survival in breast cancer cases, an effect that is independent of other risk factors. In several of the studies, the presence of a p53 mutation was the single most adverse prognostic indicator for both cancer recurrence and death (Lacroix et al., 2006). Many triple negative breast cancer (TNBC) overexpress a mutated form of p53, including the highly metathesizing model cell line MDA-MB-231 (R280K).

Therefore, restoring p53 function can be a highly effective option for cancer treatment. While functional copies of p53 can resurrect the apoptotic circuitry, it will also sensitize the tumor cells towards other various treatments (radio- and chemotherapy). Different strategies pursuing this goal have been intensively investigated, including small molecules that overcome p53 mutations and adenovirus/p53 gene delivery vectors. In 2003, China approved the first gene therapy, Gendicin, which uses p53 to treat head and neck squamous cell carcinoma (Wilson, 2005). Similar trials have been conducted in the U.S., but were discontinued due to safety concerns related to viral gene delivery. Hence, while restoring p53 functions in cancer cells has been a tantalizing approach towards combating cancer, especially for the aggressive and difficult types such as TNBC, the lack of effective delivery method has undermined its potential as an anti-cancer therapeutic.

We propose that the direct delivery of functional p53 protein into tumor cells using novel delivery vehicles can overcome current technological barriers and can be a treatment option for breast cancer, including TNBC. From a therapeutic perspective, protein-based approaches are safer than gene therapy because no random or permanent genetic changes are involved, and only transient actions of proteins are needed for the desired results. Our labs have recently developed a new and effective method of delivering proteins intracellularly, including nuclear localized transcription factors (Biswas et al., 2011; Gu et al., 2009; Zhao et al., 2011), to various human cell lines. We have demonstrated that the direct introduction of proapoptotic proteins, such as the executioner protease caspase 3 and the avian virus-derived selective tumor killer apoptin (Zhao et al., 2013), can lead to rapid resurrection of apoptosis in breast cancer cell lines and shrinkage of xenografted tumor models. **The goal of our study is to explore direct delivery of functional p53 to breast cancer cells and tumors for reactivation of apoptosis pathway.** If successful, this innovative approach can be developed into an effective treatment option for breast cancer and reduce the mortality associated with this disease. Furthermore, demonstrating the ability of intracellular protein delivery to tumor cells can facilitate the development of new tools for studying tumorgenesis and drug resistance, as well as expanding current therapeutic target pool to many other tumor suppressor proteins for cancer treatment.

2. RESULTS AND DISCUSSION

3.1. Expression, purification and refolding of recombinant p53.

The plasmid for expression of the full length human p53 protein was purchased from Addgene (Plasmid 24859). The purification and refolding of p53 was performed as described in S. Bell *et al.* Biophysical Chemistry 2002. Briefly, the plasmid was transformed into *Escherichia coli* BL21(DE3) cells and incubated at 37 °C overnight on LB agar plate with 100 μg/mL ampicillin. Colonies were picked and grown overnight at 37 °C with shaking (250 rpm) in 5 mL ampicillin-containing LB media, which were then inoculated in 500 mL of TB media with 100 μg/mL ampicillin and allowed to grow under 37 °C until the absorbance of cell density (OD_{600}) reached 0.9. Isopropyl *β*-D-1-thiogalactopyranoside (IPTG) was added to a final concentration of 0.1 mM to induce protein expression. After overnight incubation at 16 °C, the *E. coli* cells were harvested by centrifugation (3,750 rpm, 4 °C, 15 min). Cell pellets were then resuspended in 50 mL lysis buffer (0.1 mM Tris-HCl, 1mM EDTA, pH 7) and lysed by sonication. Inclusion bodies (IB) were harvested by centrifugation (31,000 *g*, 4 °C, 30 min), followed by sequential washes remove cell debris and other proteins at 4 °C (Wash 1: 60 mM EDTA, 6% triton X-100, 1.5 M NaCl, pH 7; Wash 2: 0.1 M Tris-HCl, 30 mM EDTA, 3% Triton X-100, 0.8M NaCl, pH 7; Wash 3: 0.1M Tris-HCl, 20 mM EDTA, pH 7). IB pellet was collected by centrifugation (31,000 *g*, 4 °C, 10 min) between wash buffers and was washed until a clean band of p53 can be seen on SDS-PAGE. Afterwards, the IB pellet was solubilized in solubilization buffer (100 mM Tris-HCl, 6 M Guanidinium Chloride, 50 mM DTT, pH 8) at room temperature for 2 hours. After adjusting the pH to 2 using HCl, centrifugation was used to separate solubilized p53 from any insoluble material (31,000 *g*, 4 °C, 30 min). The concentration of solubilized p53 was determined using Bradford protein assay and solubilized protein was aliquoted for -80 °C storage. Renaturation of solubilized p53 was carried out in renaturation buffer at 4 °C (50 mM Sodium Pyrophosphate, 1 M L-arginine, 2 mM DTT, 0.2 mM Zinc Chloride, pH 8). Solubilized p53 protein was diluted in renaturation buffer using step-wise addition with 90 min interval, yielding final protein concentration about 1 mg/mL. The entire renaturation volume was then dialyzed against dialysis buffer at 4 °C (50 mM Sodium Pyrophosphate, 2 mM DTT, pH 8), followed by centrifugation to remove any precipitates (31,000 *g*, 4 °C, 1 hour). The clear protein solution was concentrated and buffer exchanged into buffer containing 100 mM NaCl and 10 mM Sodium Pyrophosphate, pH 7.5. The final protein concentration was qualitatively assessed by SDS-PAGE and quantitatively determined by the Bradford protein assay. SDS-PAGE for washed pellet and p53 protein collected after final buffer exchange are shown in Figure 1 below. The secondary structure of p53 was confirmed by circular dichorism.

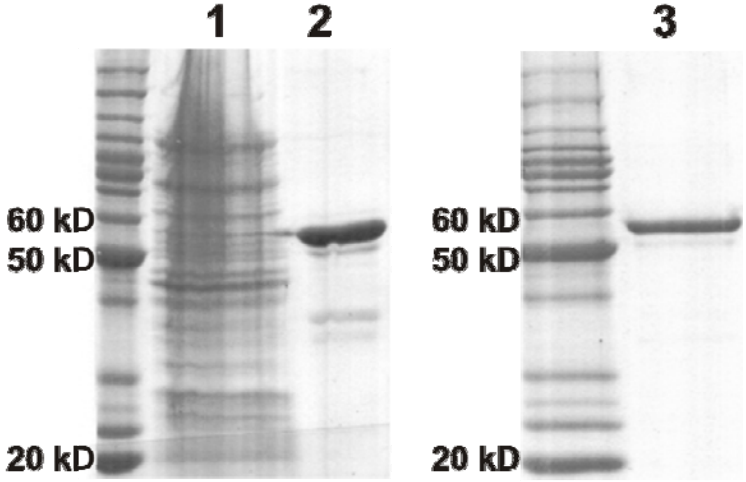

Figure 1. SDS-PAGE for p53 purification. Lane 1 proteins removed by wash buffer; Lane 2 clean IB pellet in 8 M urea; Lane 3 refolded and dialyzed p53 protein.

3.2. Synthesis of nanocapsules using p53.

A scheme for the reversible encapsulation of p53 forming redox-responsible nanocapsule (S-S p53 NC) is shown below. Monomers acrylamide (AAm) **1** and *N*-(3-aminopropyl)methacrylamide **2** (APMAAm), and

the cross-linker *N,N'*-bis(acryloyl)cystamine, at a molar ratio of 1.5:1:0.14, were first deposited onto p53 (0.7 mg) in carbonate buffer (5 mM, pH 9.0) through electrostatic forces. Then *in situ* polymerization was initiated with the addition of free radical initiators and preceded for one hour at 4 °C. The protein to monomer ratio was optimized to minimize protein precipitation during reaction, as well as to maximize the solution stability of the nanocapsule formed. Excess monomers and cross-linkers were removed using ultrafiltration and the S-S p53 NC was stored in PBS buffer (pH 7.4). Dynamic light scattering (DLS) measurement showed a shift in average diameter of the sample from ~23.44 ± 2.84 nm (native p53) to ~35.05± 1.43 nm (S-S p53 NC) with a positive ζ-potential value of 3.3±0.32 mV. The detailed size distribution of native p53 protein and S-S p53 NC formed as determined in DLS is shown in Figure 2b. TEM image of S-S p53 NC in Figure 2c revealed the particle sizes were ~ 30 nm, consistent with the sample size increase seen in DLS. These data showed that the p53 protein can be encapsulated using acrylamide-based monomers through free-radical polymerization.

We then monitored the release of p53 from such nanocapsules using ELISA assay. S-S p53 NC was first diluted into 2 µg/mL and was then incubated with 2 mM DTT for 30 minutes, 60 minutes and 90 minutes. For each time point, 2.5 µL (5 ng p53 protein/p53 NC mixture) of the incubation solution was used in ELISA assay. The incubation length was optimized to minimize loss of released p53 under elevated temperature. Using a p53 standard curve constructed with native p53 protein, the amount of p53 released from nanocapsules was calculated and plotted. Over 90 minutes of assay period, readings from DTT treated S-S p53 NC increased steadily to about ~1 ng, while control non-degradable p53 NC samples had low signals, matching signal levels of S-S p53 NC 0 minute, with very little fluctuation regardless of DTT. These results indicate that p53 is well-encapsulated inside the polymer shell and inaccessible to p53 antibody. The release of the p53 protein is indeed triggered by the presence of reducing agent and associated with the degradation of disulfide bond.

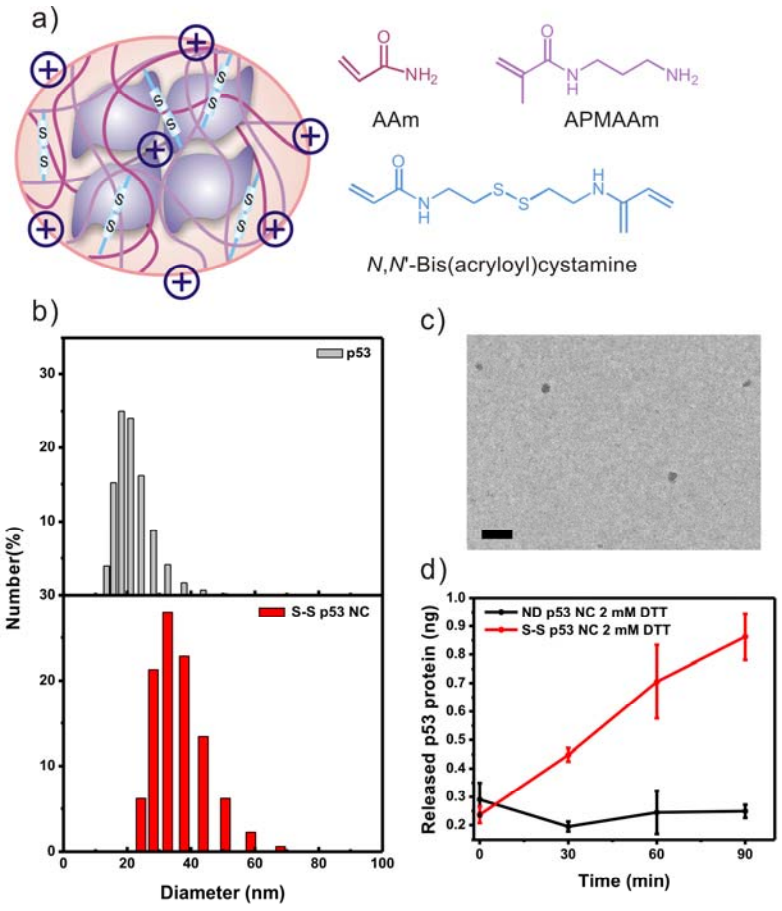

Figure 2. S-S p53 NC scheme and characterization. a) A scheme for nanocapsule and its monomers and crosslinker chemical structures; b) size distribution of native p53 protein and S-S p53 NC formed as determined in DLS; c) TEM image of S-S p53 NC. The scale bar represents 100 nm; d) ELISA assay for p53 release under reducing condition.

3.3. **Cellular uptake and localization of nanocapsules.**

To study the cellular update and protein nanocapsule localization, breast cancer cell line SK-BR-3 was incubated with S-S p53 NC. Using recombinant p53 conjugated to rhodamine dye, encapsulation was performed forming fluorescent S-S p53 NC. When added to SK-BR-3, red florescence can be seen in cells within 2 hours of incubation period, suggesting efficient cell internalization (data not shown). If internalized S-S p53 NC does protect protein until polymer shell degradation in the reducing cytosol; and encapsulation does not interfere with p53 functions, delivered p53 should be able to enter the nuclei of SK-BR-3 cells as a transcription factor. To detect whether p53 accumulates in the nuclei, SK-BR-3 was treated with S-S or ND p53 NC at a concentration of 100 ng/μL and the nuclear fraction of the cell at different time points were extracted for ELISA assay (Figure 3a). S-S p53 NC treated samples showed a clear accumulation of p53 at time points tested. Higher amount of p53 can be detected in S-S samples comparing to ND samples, though had ~2 ng nuclei p53 detected at three later time points, showed no increase of amount with increased incubation time. When treated with S-S p53 NC for various concentrations, both the cytoplasmic and nuclear fractions of SK-BR-3 cells were collected after 1 hour for determining distribution of internalized protein. With higher S-S p53 NC concentrations, much higher amount of p53 can be detected in the cytoplasmic fraction. More p53 in nucleus fraction can also be detected as concentration increases, but not as dramatic as cytoplamic fractions possible due to slower nuclear transport than cellular internalization. The nucleus accumulation of p53 delivered in S-S NC can also be visualized by taking confocal images of MDA-MB-231 cells incubated with rhodamine-conjugated p53 NC, shown in Figures 3c and 3d. Together, the results indicated that p53 NC can be efficiently internalized into cells, where the polymer shell degrades to release p53 cargo. Released p53 protein was able to locate in the nuclei of cells in a concentration- and time-dependent manner.

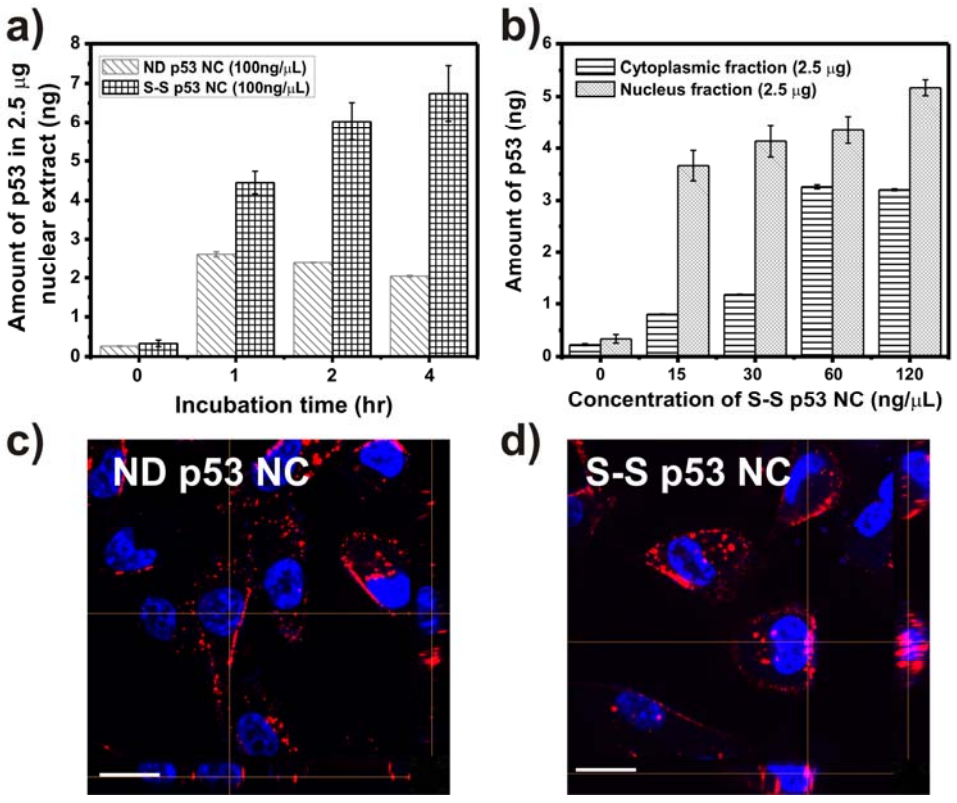

Figure 3. Cellular uptake of nanocapsule and localization of released protein. a) ELISA of nuclear fraction of SK-BR-3 cells treated with 100ng/μL S-S and ND p53 NC for 0, 1, 2, and 4 hours; b) ELISA of cytoplasmic and nuclear fraction of SK-BR-3 cells treated with S-S p53 NC 1 hours; c) Confocal image of MDA-MB-231 with ND p53 NC; d) Confocal image of MDA-MB-231 with S-S p53 NC. The scale bar represents 20 μm. Nuclei is stained with DAPI.

We next tested cytotoxicity of the p53 delivered by using three different cancer cell lines, MDA-MB-231, SK-BR-3, and BT-474. S-S p53 NC reduced viable cell percentage dramatically with IC_{50} values ~ 200 nM. ND p53 NC and native p53 protein were included as negative controls, which did not affect any of viability on the cell lines tested as expected (Figure 4a-c).

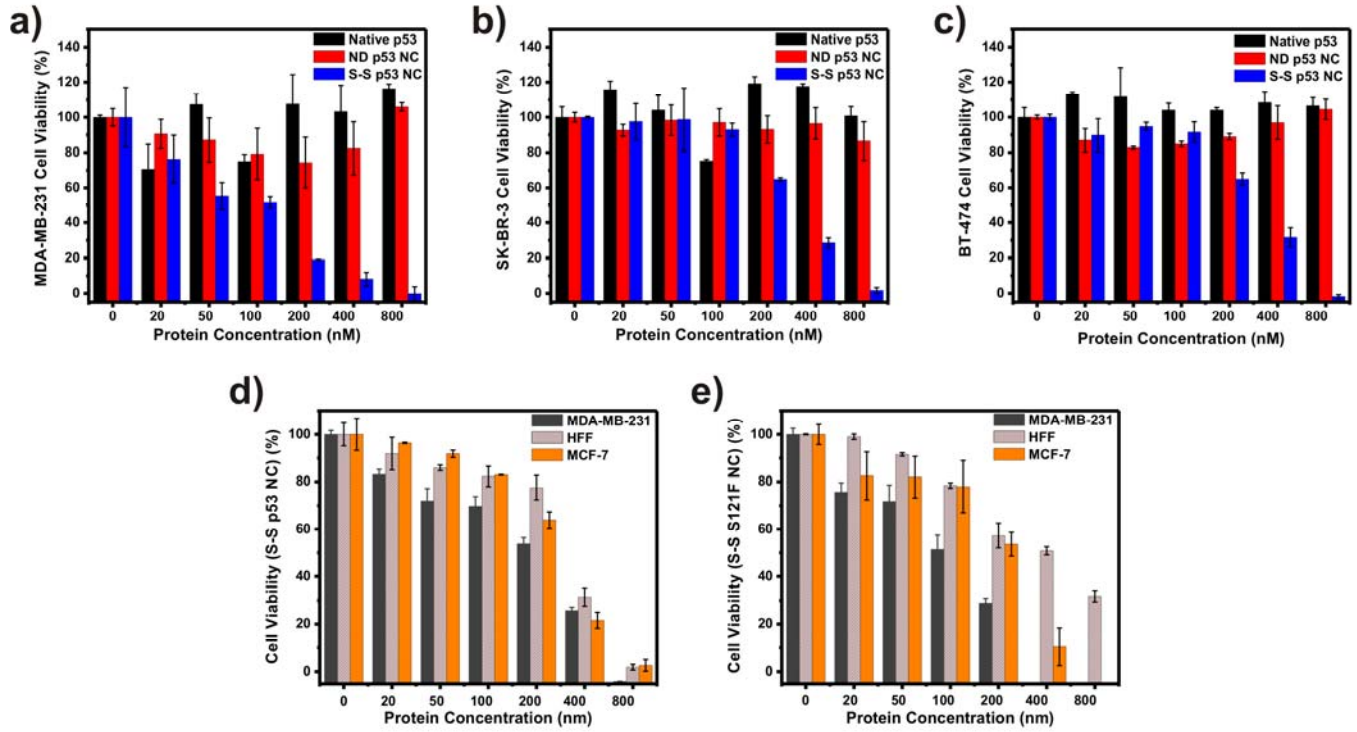

Figure 4. Cytotoxicity of wild-type and pro-apoptotic mutant p53 delivered by S-S NC .

Some of the p53 mutants have a higher apoptotic activity than WT p53. Also improvements can be made to stabilize p53 by engineering out the Mdm2 binding site or alterations to favor the induction of apoptotic genes. One example of these gain-of-function mutants is S121F and there are at least another 17 mutants expressing higher apoptotic activity, with an increased affinity for some p53-binding sites. The apoptotic function requires transcription activation by p53. The S121F mutant has altered sequence specificity and selectively fails to activate MDM2 transcription, which decreases MDM2 feedback control and increases or unbalance the expression of apoptotic target genes. In the same study, it was also shown that the mutant S121F failed to kill wild-type mouse embryo fibroblasts. To test the delivery and potential tumor-cell selectivity of the "super-p53", we introduced the mutation S121F using site-directed mutagenesis and express the mutant p53 S121F in *E. coli*. The mutant was similarly encapsulated by the interfacial polymerization approach and administered to different cells line to measure the cytotoxicity. Wild type p53 NC were used side by side for comparison purpose (Figures 4d and 4e). We used the breast cancer cell lines MDA-MB-231 (TNBC) and MCF7, together with noncancerous cell line, human foreskin fibroblast (HFF). MTS assays will be performed to compare the effect of WT p53 NCs vs. the super p53 mutant S121F NCs toward these cell lines. As can be seen in Figure 4d, the wild type p53 induced apoptosis in all three cell lines with equal potency, while the super p53 NC not only induced apoptosis in cancer cells at lower concentration, but also left higher amount of HFF cells unaffected. Therefore, our approach was able to capture the improved properties of the S121F mutant, and this mutant NC formulation will be used in the upcoming animal experiments.

3.4. Develop new crosslinking chemistry.

A critical and often essential feature of effective chemotherapy is tumor specificity. Even though passive accumulation through the "leaky vasculature" of the tumor does occur, it is much more desirable to achieve direct targeting of the breast cancer tumors. Outfitting the anticancer agent with targeting ligands will not only decrease the toxicity to healthy tissues, but also result in higher local concentration of the agent near

the tumor site, resulting in maximum dosage to the tumor. Therefore, an important objective of this proposal is to decorate the surface of the protein nanocapsules with ligands that can confer breast cancer selectivity.

The surface of the nanocapsule can be easily modified with mild chemistry, thereby allowing the conjugation of different moieties without compromising the integrity of the nanocapsule and the cargo inside. Furthermore the monomer can be itself functionalized to allow post-encapsulation modification. We have recently demonstrated this is feasible as shown in Figure 5. To do so, we replaced the positively charged monomer **2** with an azide containing AzPEG-AAm monomer. Upon polymerization the net surface charge is neutral, thereby making the nanocapsules unable to penetrate cell membrane passively. However, the incorporated azide group allows conjugation to alkyne containing ligand using "Click" chemistry (Lallana et al., 2012). The ligand itself can be prepared by conjugation to the cyclooctyne DBCO-PEG4-NHS ester under aqueous conditions. Following "clicking" the ligand onto the surface of the nanocapsule, the nanocapsule is can now be internalized into target cells through receptor mediated endocytosis specific for the attached ligand. To demonstrate this is possible, we conjugated the luteinizing hormone releasing hormone (LHRH) peptide to GFP nanocapsules (Zhang and Xu, 2011). As shown in Figure 4, GFP fluorescence can only be detected in cell lines that overexpress LRHR receptor, such as MB-MDA-231, but not in those that do not express the receptor, such as SK-OV3 (See Figure 5 Legend). This illustrates the conjugation and targeting steps are all effective.

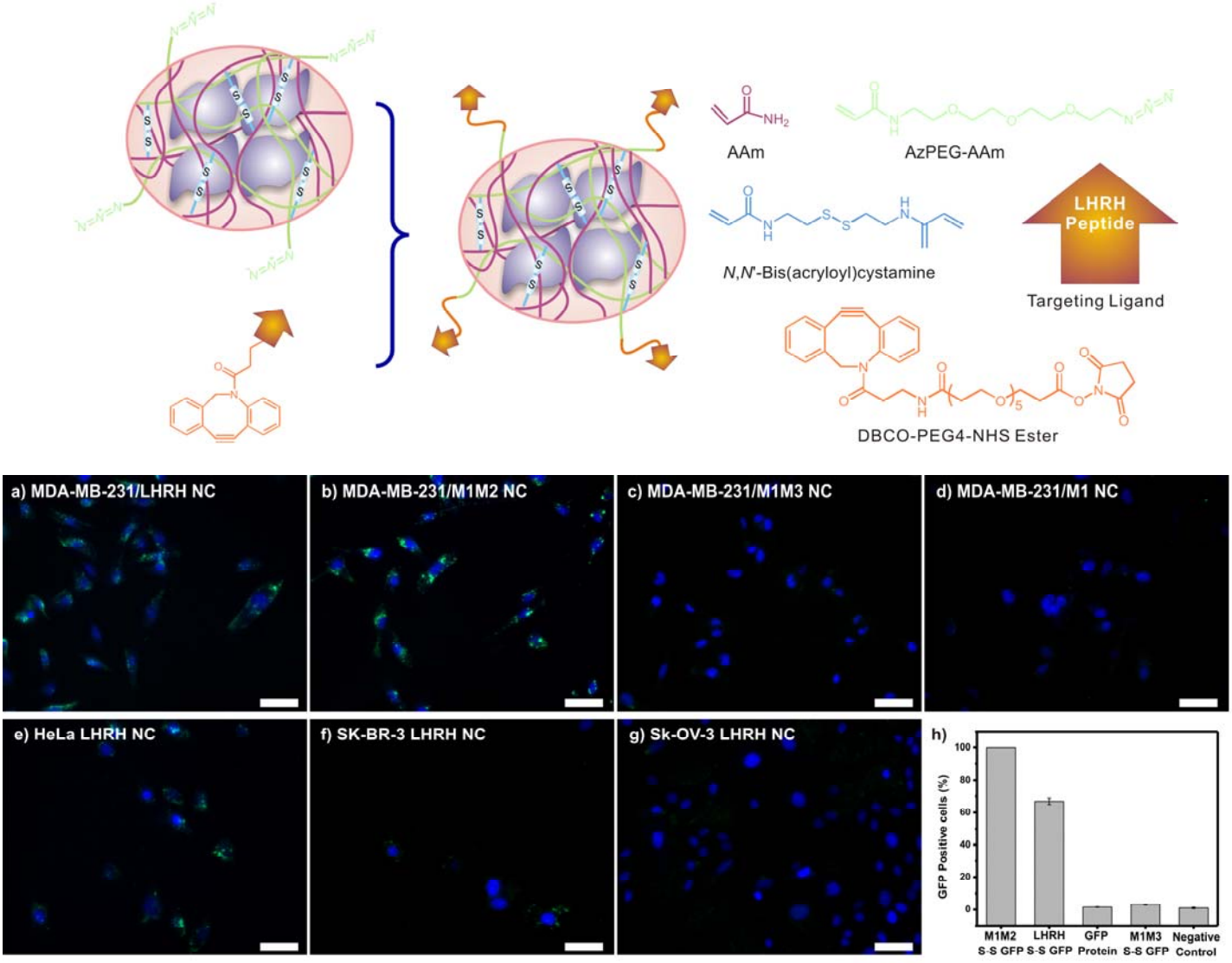

Figure 5. (Top) Strategy to couple targeting ligands to the surface of NCs using click chemistry; (Bottom) comparing the internalization efficiency of cells towards LHRH-coupled eGFP NCs. Strongest internalization is observed in HeLa, MDA-MB-231 and SK-BR3 cells line that overexpress the LHRH receptor. If LHRH peptide is not conjugated to the surface of the NCs, no internalization is observed. Similarly, no internalization was detected in SK-OV3 cell line, which does not overexpress the LHRH receptor. In (h), although the overall internalization efficiency is lower for LHRH tagged NC compared to positively charged NCs, the selectivity is desirable.

Next, to test the selectivity of the LHRH tagged S121F p53 towards only the breast cancer cell lines that overexpress the surface receptor, we measured the relative toxicity of the particles in the presence of three cell lines (MDA-MB-231, which overexpressed LHRH receptor; SK-OV3, an ovarian cancer cell line that does not express the LHRH peptide; and HFF, a noncancerous cell line that does not overexpress the receptor). As can be seen in Figure 6, the LHRH tagged S121F p53 only killed the TNBC cell line that overexpresses LHRH receptor. In sharp contrast, other two cells lines remain largely unaffected. The cytotoxicity towards MDA-MB-231 is also solely from the p53 cargo, as using a LHRH-tagged eGFP NC did not lead to cell death.

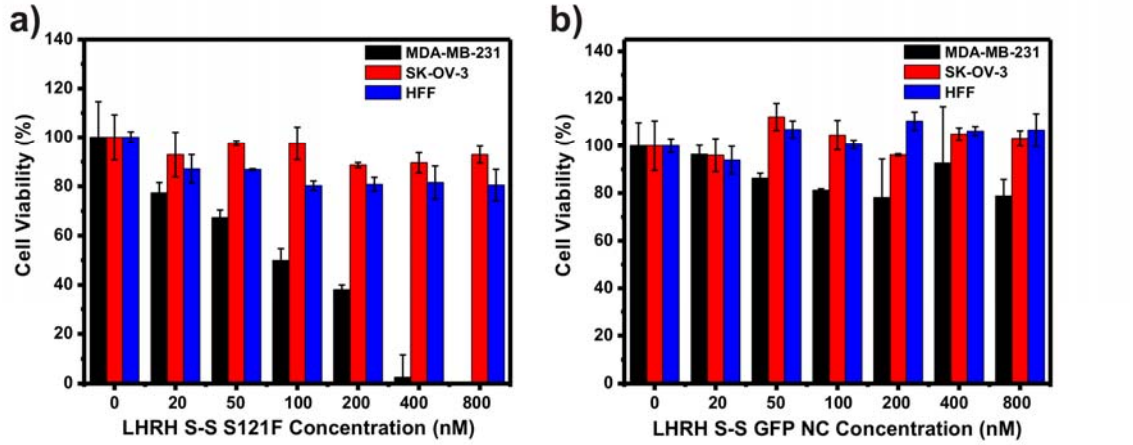

Figure 6. Tumor cell line selectivity of the LHRH tagged p53 S121F NCs.

KEY RESEARCH ACCOMPLISHMENTS

- We synthesized polymer nanocapsules for delivery of the cellular guardian transcription factor p53
- The nanocapsule can be internalized by different tumor cells and the protein cargo is released intracellularly in response to the reducing environment of the cytoplasm.
- A new conjugation method of a targeting peptide to the surface of nanocapsules is developed.

REPORTABLE OUTCOMES

Publications:

Zhao, M., Hu, B., Gu, Z., Joo, K., Wang, P., Tang, Y. "Degradable Polymeric Nanocapsule for Efficient Intracellular Delivery of a High Molecular Weight Tumor-Selective Protein Complex." *Nano Today.* **2013**, 8, 11-20

Presentations in this period:

The PI Tang has made the following presentations in which this material has been included.

Department of Bioengineering, Rice University, January 2013

Society of Biological Engineering 4th International Conference on Biomolecular Engineering, Invited Speaker, Ft. Lauderdale, Florida, January 2013

The following presentation was made by Muxun Zhao, the graduate student involved in this project.

American Institute of Chemical Engineers Annual Meeting, Pittsburgh, Oral Presentation: RedoxResponsive Polymeric Nanocapsules for Protein Delivery. November 2012

Society of Biomaterials Annual Meeting, Boston, Poster presentation: Redox-Responsive Polymeric Nanocapsules for Protein Delivery. April 2013

CONCLUSION

During this period we demonstrated that p53 (and the super p53) is an attractive antitumor protein targeting breast cancer cell lines. We also introduced a new polymerization technique that allows selective modification of the NC with targeting ligands through the bioorthogonal click chemistry. With these two accomplishments, we are now moving towards animal experiments using S121 NCs outfitted with LHRH ligands. We envision a intravenous administered NC will be able to control and eliminate tumor growth.

REFERENCES

Biswas, A., Joo, K.I., Liu, J., Zhao, M., Fan, G., Wang, P., Gu, Z., and Tang, Y. (2011). Endoprotease-mediated intracellular protein delivery using nanocapsules. ACS Nano *5*, 1385-1394.

Coles, C., Condie, A., Chetty, U., Steel, C.M., Evans, H.J., and Prosser, J. (1992). p53 mutations in breast cancer. Cancer Res *52*, 5291-5298.

Cotter, T.G. (2009). Apoptosis and cancer: the genesis of a research field. Nat Rev Cancer *9*, 501-507.

Gu, Z., Yan, M., Hu, B., Joo, K.I., Biswas, A., Huang, Y., Lu, Y., Wang, P., and Tang, Y. (2009). Protein nanocapsule weaved with enzymatically degradable polymeric network. Nano Lett *9*, 4533-4538.

Lacroix, M., Toillon, R.A., and Leclercq, G. (2006). p53 and breast cancer, an update. Endocr Relat Cancer *13*, 293-325.

Lallana, E., Fernandez-Trillo, F., Sousa-Herves, A., Riguera, R., and Fernandez-Megia, E. (2012). Click chemistry with polymers, dendrimers, and hydrogels for drug delivery. Pharmaceutical research *29*, 902-921.

Wilson, J.M. (2005). Gendicine: the first commercial gene therapy product. Hum Gene Ther *16*, 1014-1015.

Wu, M.A., Jiang, P., Du, W.J., Wang, X.W., Mancuso, A., Gao, X.A., and Yang, X.L. (2011). p53 regulates biosynthesis through direct inactivation of glucose-6-phosphate dehydrogenase. Nat Cell Biol *13*, 310-U278.

Zhang, X., and Xu, C. (2011). Application of reproductive hormone peptides for tumor targeting. Current pharmaceutical biotechnology *12*, 1144-1152.

Zhao, M., Biswas, A., Hu, B., Joo, K.I., Wang, P., Gu, Z., and Tang, Y. (2011). Redox-responsive nanocapsules for intracellular protein delivery. Biomaterials *32*, 5223-5230.

Zhao, M.X., Hu, B.L., Gu, Z., Joo, K.I., Wang, P., and Tang, Y. (2013). Degradable polymeric nanocapsule for efficient intracellular delivery of a high molecular weight tumor-selective protein complex. Nano Today *8*, 11-20.

APPENDICES

Publication from this period

Zhao, M., Hu, B., Gu, Z., Joo, K., Wang, P., Tang, Y.† "Degradable Polymeric Nanocapsule for Efficient Intracellular Delivery of a High Molecular Weight Tumor-Selective Protein Complex." *Nano Today.* **2013**, 8, 11-20.

Nano Today (2013) 8, 11—20

Available online at www.sciencedirect.com

SciVerse ScienceDirect

journal homepage: www.elsevier.com/locate/nanotoday

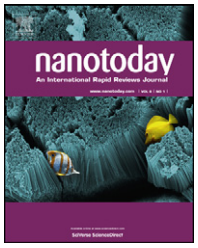

RAPID COMMUNICATION

Degradable polymeric nanocapsule for efficient intracellular delivery of a high molecular weight tumor-selective protein complex

Muxun Zhao[a], Biliang Hu[b], Zhen Gu[a,1], Kye-Il Joo[b], Pin Wang[b,], Yi Tang[a,c,*]**

[a] *Department of Chemical and Biomolecular Engineering, University of California, Los Angeles, CA 90095, USA*
[b] *Mork Family Department of Chemical Engineering and Materials Science, University of Southern California, Los Angeles, CA 90089, USA*
[c] *California NanoSystems Institute, University of California, Los Angeles, CA 90095, USA*

Received 29 May 2012; received in revised form 4 November 2012; accepted 26 December 2012
Available online 1 February 2013

KEYWORDS
Nanogel;
Core—shell;
Redox-responsive;
Apoptosis;
Breast cancer

Summary The development of stimuli-responsive, nano-scale therapeutics that selectively target and attack tumors is a major research focus in cancer nanotechnology. A potent therapeutic option is to directly arming the cancer cells with apoptotic-inducing proteins that are not affected by tumoral anti-apoptotic maneuvers. The avian virus-derived apoptin forms a high-molecular weight protein complex that selectively accumulates in the nucleus of cancer cell to induce apoptotic cell death. To achieve the efficient intracellular delivery of this tumor-selective protein in functional form, we synthesized degradable, sub-100 nm, core—shell protein nanocapsules containing the 2.4 MDa apoptin complexes. Recombinant apoptin is reversibly encapsulated in a positively charged, water soluble polymer shell and is released in native form in response to reducing conditions such as the cytoplasm. As characterized by confocal microscopy, the nanocapsules are efficiently internalized by mammalian cells lines, with accumulation of rhodamine-labeled apoptin in the nuclei of cancer cells only. Intracellularly released apoptin induced tumor-specific apoptosis in several cancer cell lines and inhibited tumor growth *in vivo*, demonstrating the potential of this polymer—protein combination as an anticancer therapeutic.

Abbreviations: NC, nanocapsule; APO, apoptin; S—S, disulfide bonded; AAm, acrylamide; APMAAm, *N*-(3-aminopropyl)methacrylamide; MBP, maltose binding protein; Rho, rhodamine; ND, nondegradable; HFF, human foreskin fibroblast.

* Corresponding author at: 420 Westwood Plaza, Los Angeles, CA 90095, USA. Tel.: +1 310 825 0375; fax: +1 310 206 4107.
** Corresponding author at: 925 Bloom Walk, HED 216, Los Angeles, CA 90089, USA. Tel.: +1 213 740 0780; fax: +1 213 740 7223.
E-mail addresses: pinwang@usc.edu (P. Wang), yitang@ucla.edu (Y. Tang).
[1] Current address: Joint Department of Biomedical Engineering, University of North Carolina at Chapel Hill, North Carolina State University, Raleigh, NC 27606, USA.

1748-0132/$ — see front matter © 2013 Elsevier Ltd. All rights reserved.
http://dx.doi.org/10.1016/j.nantod.2012.12.003

Introduction

The most desirable anticancer therapy is both potent and specific toward tumor cells [1,2]. Many conventional small molecule chemotherapeutics do not discriminate between cancerous and normal cells, cause damage to healthy tissues, and are therefore unable to be administered at high dosage. In contrast, cytoplasmic and nuclear proteins that selectively alter the signaling pathways in tumor cells, reactivate apoptosis and restore tissue homeostasis, can delay tumor progression with less collateral damage to other tissues [3—6]. Using stimuli-responsive nanocarriers for the intracellular delivery of such proteins, including human tumor suppressors [7] and exogenous tumor-killing proteins [8—10]), is attractive as a new anti-cancer therapy modality.

Apoptin is a 121-residue protein derived from chicken anemia virus [9]. When transgenically expressed, apoptin can induce p53-independent apoptosis in a variety of tumor and transformed cells [11,12], while leaving normal and untransformed cells unaffected [13]. Apoptin exists as a globular multimeric complex, composed of thirty to forty subunits, with no well-defined secondary structure [14]. While the exact mechanism of the tumor selectivity is unresolved, apoptin is known to translocate to the nucleus where tumor-specific phosphorylation at residue Thr108 takes place, leading to accumulation of apoptin in nucleus and activation of the apoptotic cascade in tumor cell [15]. In normal cells, apoptin is not phosphorylated at Thr108 and is located mostly in the cytoplasm, where it aggregates and undergoes degradation [16]. Because of the high potency in inducing this exquisite tumor-selective apoptosis, apoptin has been investigated widely as an anti-tumor therapeutic option [9]. Different gene therapy approaches have been used to administer apoptin to mouse xenograft tumor models, in which significant reduction in tumor sizes and prolonged lifespan of mice have been observed without compromising the overall health [17—19]. However, as with other gain-of-function therapy candidates, *in vivo* gene delivery approaches using viral vectors may lead to unwanted genetic modifications and elicit safety concerns [20]. While protein transduction domain (PTD)-fused apoptin has been delivered to cells [21,22], this approach suffers from inefficient release of the cargo from endosomes and instability of the unprotected protein [23]. Development of nanoparticle carriers to aid the functional delivery of apoptin to tumor cells is therefore desirable [24].

We chose to work with recombinant maltose-binding-protein fused apoptin (MBP—APO) that can be solubly expressed from *Escherichia coli*, whereas native apoptin forms inclusion bodies [14]. MBP—APO has been shown to similarly assemble into a multimeric protein complex, which exhibits the essential functions and selectivity of native apoptin [14]. Nanoparticle-mediated delivery of functional MBP—APO poses unique challenges [25]. First, MBP—APO preassembles into large complex with an average diameter of ~40 nm and molecular weight of ~2.4 MDa [14]. To achieve nanocarrier sizes that are optimal for *in vivo* administration (~100 nm) [26], a loading strategy that forms compact particles is desirable. Second, in order to maintain the multimeric state of functional MBP—APO, the protein loading and releasing steps need to take place under very mild, physiological conditions in the absence of surfactants. Lastly, the nanocarrier must completely disassemble inside the cell to release the MBP—APO in its native and unobstructed form to ensure the correct spatial presentation of key residues within the apoptin portion, including the nuclear localization/export signals, the phosphorylation site and other elements important for downstream signaling.

In the current study, we selected a polymeric nanocapsule (NC) strategy for the functional delivery of MBP—APO, in which the protein complex is noncovalently protected in a water soluble polymer shell (Fig. 1). This slightly positively charged shell shields the MBP—APO from serum proteases and surrounding environment, while enabling cellular uptake of the polymer—protein complex through endocytosis [27]. The polymeric layer is weaved together by redox-responsive cross-linkers containing disulfide bond (S—S) that can be degraded once the NCs are exposed to the reducing environment in cytoplasm [28]. No covalent bonds are formed between the protein cargo and the polymer shell, which ensures complete disassembly of the capsule layer and release of native MBP—APO inside the cell. Using this approach, we show that MBP—APO can be efficiently delivered to induce apoptosis in cancer cell lines selectively both *in vitro* and *in vivo*.

Materials and methods

Materials

N-(3-aminopropyl)methacrylamide hydrochloride was purchased from Polymer Science, Inc. CellTiter 96® AQueous One Solution Cell Proliferation Assay (MTS) reagent was purchased from Promega Corporation. APO-BrdU™ TUNEL Assay Kit was purchased from Invitrogen. *In Situ* Cell Death Detection Kit, POD; was purchased from Roche Applied Science. Female athymic nude (*nu*/*nu*) mice, 6 weeks of age, were purchased from Charles River Laboratories (Wilmington, MA). All other chemicals were purchased from Sigma—Aldrich and used as received.

Protein nanocapsule preparation

The concentration of protein was diluted to 1 mg/mL with 5 mM sodium bicarbonate buffer at pH 9. Then 200 mg/mL acrylamide (AAm) monomer was added to 1 mL of protein solution with stirring at 4 °C. After 10 min, the second monomer, *N*-(3-aminopropyl)methacrylamide (APMAAm), was added while stirring. Different cross-linkers, *N*,*N*′-methylene bisacrylamide for ND NC and *N*,*N*′-bis(acryloyl)cystamine for S—S NC, were added 5 min after the addition of APMAAm. The polymerization reaction was immediately initiated by adding 30 μL of ammonium persulfate (100 mg/mL, dissolved in deoxygenated and deionized water) and 3 μL of *N*,*N*,*N*′,*N*′-tetramethylethylenediamine. The polymerization reaction was allowed to proceed for 60 min. The molar ratios of AAm/APMAAm/cross-linker used were

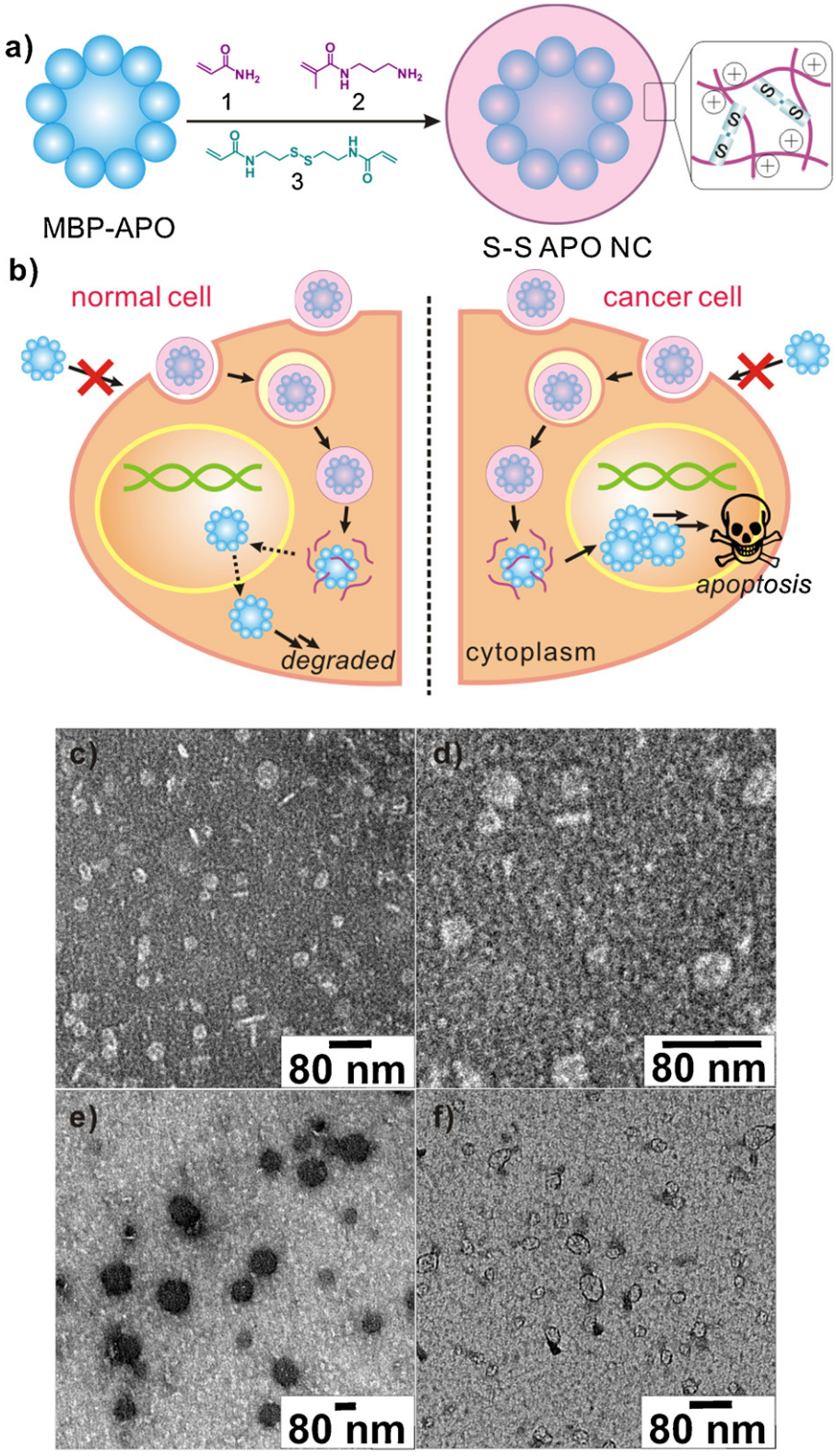

Figure 1 Degradable nanocapsules for apoptin delivery. (a and b) Schematic diagram of synthesis of degradable apoptin nanocapsules (S—S APO NC) and delivery into tumor cells to induce apoptosis; TEM images of (c) native MBP—APO; (d) enlarged image of MBP—APO; (e) S—S APO NC; and (f) degraded S—S APO NC after treatment with 2 mM GSH for 6 h at 37 °C.

1.5:1:0.14, 2:1:0.14, 4:1:0.14, and 8:1:0.14. Buffer exchange with phosphate-buffered saline (PBS) buffer (pH 7.4) was used to remove the remaining monomers and initiators. Rhodamine-labeled APO NCs was obtained through encapsulation of MBP—APO modified with 5-carboxy-X-rhodamine *N*-succinimidyl ester (mass ratio (MBP—APO:rhodamine) = 4:1).

Characterization of protein nanocapsules

The mean hydrodynamic size and ζ-potential of NC were determined by dynamic light scattering (DLS) in PBS buffer. Samples of NCs (0.05 mg/mL) for TEM imaging were negatively stained with 2% uranyl acetate in alcoholic solution (50% ethanol). The lamella of stained sample was prepared on carbon-coated electron microscopy grids (Ted Pella, Inc.).

Cellular uptake and localization of nanocapsules

MDA-MB-231, HeLa, MCF-7, and human foreskin fibroblast (HFF) cells (ATCC, Manassas, VA) were cultured in Dulbecco's modified Eagle's media (DMEM) (Invitrogen) supplemented with 10% bovine growth serum (Hyclone, Logan, UT), 1.5 g/L sodium bicarbonate, 100 μg/mL streptomycin and 100 U/mL penicillin, at 37 °C with 98% humidity and 5% CO_2. To visualize NCs uptake, MDA-MB-231 cells were seeded into 48-well plate, with a density of 10,000 cells/well in 250 μL of media with supplements. S—S Rho—APO NC and ND Rho—APO NC were added to a final concentration of 20 nM. After 1 h and 24 h of incubation, cells were washed with PBS twice, stained with DAPI Nucleic Acid Stain and imaged. For internalization of S—S Rho—APO NC with different ζ-potentials, MDA-MB-231 cells were incubated with 20 nM NCs for 2 h before nuclei staining. Markers for early and late endosomes were used for internalization trafficking study. A concentration of 20 nM S—S Rho—APO NCs was added to HeLa cells and incubated for 30 min, 60 min and 120 min under 37 °C. Cells were then fixed with 4% formaldehyde, permeabilized with 0.1% Triton X-100, and stained with antibodies, mouse anti-EEA1 antibody against early endosomes and rabbit anti-CI-MPR antibody against late endosomes (Cell Signaling Technology, Inc.). Texas red goat anti-mouse IgG and Alexa Fluor® 647 goat anti-rabbit IgG (Invitrogen) were added as the secondary antibody. To determine the cellular localization of the protein delivered, confocal images were taken with HeLa, MCF-7, and HFF cells incubated with 20 nM of S—S Rho—APO NC or ND Rho—APO NC at 37 °C for 24 h. Nuclei were then counterstained with DAPI. The Z-stack images of cells were imaged at 0.4-μm intervals and analyzed by Nikon NIS Element software. Fluorescent microscopy images were acquired on a Yokogawa spinning-disk confocal scanner system (Solamere Technology Group, Salt Lake City, UT) using a Nikon eclipse Ti-E microscope equipped with a 60×/1.49 Apo TIRF oil objective and a Cascade II: 512 EMCCD camera (Photometrics, Tucson, AZ, USA). An AOTF (acousto-optical tunable filter) controlled laser-merge system (Solamere Technology Group Inc.) was used to provide illumination power at each of the following laser lines: 491 nm, 561 nm, and 640 nm solid state lasers (50 mW for each laser).

Cytotoxicity assays

Different cancer cells lines, HeLa, MCF-7 and MDA-MB-231, as well as noncancerous HFF, were seeded into 96-well plates, each well containing 5000 cells in 100 μL of DMEM with supplements. Different concentrations of protein and NCs were added into each well and the plates. After incubation of 48 h at 37 °C, the wells were washed with PBS solution twice and 100 μL of fresh cell culture media with supplements was added. Then 20 μL MTS solution (CellTiter 96® AQueous One Solution Cell Proliferation Assay) was added into each well and the plates were incubated for 3 h at 37 °C. The absorbance of each well was read at 490 nm using a microplate reader (PowerWave X, Bio-tek Instruments, USA). Apoptosis was detected using APO-BrdU Terminal Deoxynucleotidyl Transferase dUTP Nick End Labeling (TUNEL) assay kit. MDA-MB-231 and HFF cells were seeded at a density of 100,000 cells/well into a 6-well plate in 2 mL of cell culture media with supplements. Proteins and NCs were added after cells covered 80% of bottom surface. After 24 h of incubation, cells were fixed with 1% paraformaldehyde in PBS, followed by the addition of DNA labeling solution containing terminal deoxynucleotidyl transferase and bromodeoxyuridine (BrdUrd). Cells were then stained with Alexa Fluor® 488 dye-labeled anti-BrdUrd antibody. Samples were deposited onto slides, which were later stained with propidium iodide (PI) solution containing RNase A. Images were obtained by fluorescent microscope (Zeiss, Observer Z1) using appropriate filters for Alexa Fluor 488 and PI.

In vivo studies with MCF-7 xenograft model

All mice were housed in an animal facility at the University of Southern California in accordance with institute regulations. Female athymic nude (*nu*/*nu*) mice were subcutaneously grafted on the back flank with 5×10^6 MCF-7 tumor cells. Afterwards, tumor size was monitored by a fine caliper and the tumor volume was calculated as the product of the two largest perpendicular diameters and the vertical thickness ($L \times W \times D$, mm^3). When the tumor volume reached 100—200 mm^3, mice were randomly separated into different groups. From day 0, mice were treated with intratumoral injection of native MBP—APO or S—S APO NC (200 μg per mouse) every other day. PBS and S—S BSA NC were included as the negative controls. When the tumor volume exceeded 2500 mm^3, the mice were euthanized by CO_2 according animal protocol. The average of tumor volumes was plotted as the tumor growth curve in respective treated groups. For histology study, treated tumor samples were collected and fixed in 4% paraformaldehyde, and processed for staining using the *In Situ* Cell Death Detection Kit. The stained tumor slides were observed under microscope, and representative pictures were taken for analysis. Paraformaldehyde-postfixed frozen tumor sections (5-μm thick) were permeabilized with 0.1% triton X-100 and stained with TUNEL assay kit (*In Situ* Cell Death Detection Kit, POD; Roche Applied Science, Indianapolis, IN) in accordance with

the manufacturer's instructions. DAPI was used for nuclear counterstaining.

Results and discussion

Synthesis and characterization of apoptin nanocapsules

MBP—APO (p*I* = 6.5) was first purified from *E. coli* extract using an amylose-affinity column (Supplement 2 and Supplement 8). Dynamic light scattering (DLS) measurement revealed an average hydrodynamic radius of 36.1 nm (Supplement 3), consistent with the reported size for the recombinant MBP—APO complex [14]. Transmission electron microscopy (TEM) analysis of MBP—APO showed similarly sized protein complexes (Fig. 1c and enlarged in Fig 1d). Interestingly, MBP—APO complexes appear to adopt a disk-shaped structure despite the lack of defined secondary structure from the apoptin component. Since the apoptin portion of the protein can self-assemble into the ~40-mer complex, we propose a three dimensional arrangement of MBP—APO in which the C-terminal apoptin forms the central spoke of the wheel-like structure (Fig. 1a), with the larger MBP portion distributes around the apoptin. The planar arrangement allows the apoptin portion of the fusion protein to remain accessible to its protein partners, which may explain how the MBP—APO fusion retains essentially all of the observed functions of native apoptin.

The reversible encapsulation strategy for producing apoptin NCs is shown in Fig. 1a. Following electrostatic deposition of the monomers acrylamide (**1** in Fig. 1a) and *N*-(3-aminopropyl)methacrylamide (**2**), and the cross-linker *N*,*N*′-bis(acryloyl)cystamine (**3**), at a molar ratio of 1.5:1:0.14, onto MBP—APO (1 mg) in carbonate buffer (5 mM, pH 9.0), *in situ* polymerization was initiated with the addition of free radical initiators and proceeded for 1 h. The molar ratio and the time of reaction reported were optimized to minimize protein aggregation and precipitation, as well as to maximize the solution stability of the resulting NCs (designated below as S—S APO NC). Excess monomers and cross-linkers were removed using ultrafiltration and S—S APO NC was stored in PBS buffer (pH 7.4). DLS clearly showed increase in average diameter of the sample to ~75 nm (Supplement 3) with a slightly positive ζ-potential value of 2.8 mV (Supplement 1). TEM analysis of the S—S APO NC confirmed the nearly doubling in diameter of the spherical particle (Fig. 1e). Unexpectedly, the NCs displayed dark contrast upon uranyl acetate staining, which hints that the cores of the particles were very densely packed. As expected from the incorporation of redox-responsive cross-linker **3**, the reduction of NCs size can be seen upon treatment of the reducing agent glutathione (GSH) (2 mM, 6 h, 37 °C). As shown in Fig. 1f, the densely packed NCs were completely dissociated into ~30 nm particles, confirming the reversible nature of the encapsulation process. As a control, we also synthesized nondegradable MBP—APO NCs (ND APO NC) using *N*,*N*′-methylene bisacrylamide as the cross-linker with same monomer and protein concentrations under identical reaction conditions. Whereas similarly sized NCs were formed, no degradation of ND APO NC can be observed in the presence of GSH.

Cellular uptake and localization of nanocapsules

We next examined the cellular uptake of the S—S APO NC and cellular localization of the cargo. If the unique tumor selectivity of MBP—APO is maintained following the encapsulation and release processes, we expect the delivered MBP—APO to either accumulate in the nuclei of the tumor cells, or to localize in the cytoplasm of noncancerous cells. Prior to the polymerization process, the MBP—APO protein was conjugated to amine-reactive rhodamine (Rho—APO) as described in section 'Protein nanocapsule preparation'. Subsequent encapsulation yielded similarly sized NCs as unlabeled S—S APO NCs. Fluorescent microscopy showed all NCs readily penetrated the cell membrane and are present in the cytoplasm of MDA-MB-231 cells within 1 h (Supplement 4). When the relative amounts of positively charged monomer **2** were reduced in the NC shell, corresponding decreases in ζ-potentials of the NCs were measured by DLS, which led to decreases in cellular internalization (Supplement 5). The cellular trafficking of the internalized S—S Rho—APO NCs in HeLa cells was investigated for 2 h by monitoring colocalization using fluorescent markers for early and late endosomes (Fig. 2a and Supplement 6). Colocalization of Rho—APO with early endosomes was detected at the highest levels after 30 min and decreased at later time points. In contrast, colocalization of Rho—APO with late endosome remained low throughout the trafficking studies. Colocalization of Rho—APO with nuclei became evident after 2 h, indicating endosomal escape and nuclear entry of the released apoptin protein. These results suggested that S—S Rho—APO NCs were trafficked into early endosomes upon internalization and at least a significant portion of the internalized NCs and the cargo can escape from the endosomal compartment.

To analyze protein localization using confocal microscopy, two cancer cell lines HeLa and MCF-7, together with the noncancerous human foreskin fibroblast (HFF), were treated with either S—S Rho—APO NC or ND Rho—APO NC (Fig. 2b). In the case of ND Rho—APO NCs, red fluorescence signals remained in the cytoplasm for all three cell lines, indicating the encapsulated Rho—APO proteins were well-shielded by the nondegradable polymer shell and the internal nuclear localization sequences were not accessible to the transport machinery. In stark contrast, when HeLa cells were treated with S—S Rho—APO NC, strong red fluorescence of rhodamine was present in the nuclei, resulting in intense pink color as a result of overlapping of rhodamine and DAPI fluorescence. Z-stacking analysis confirmed the Rho—APO to be localized inside of the nuclei. Similar results were observed with MCF-7 cells, although the fluorescence intensity was not as strong as in the HeLa cells. These results confirmed that the Rho—APO delivered can indeed be released in native forms inside the cytoplasm and enter the nuclei. More importantly, the tumor-specificity of delivered apoptin proteins toward cancer cell lines were demonstrated in the confocal analysis of noncancerous HFF cells treated with S—S Rho—APO NC, as all of the dye signals remained in the cytoplasm and no nuclear accumulation was observed.

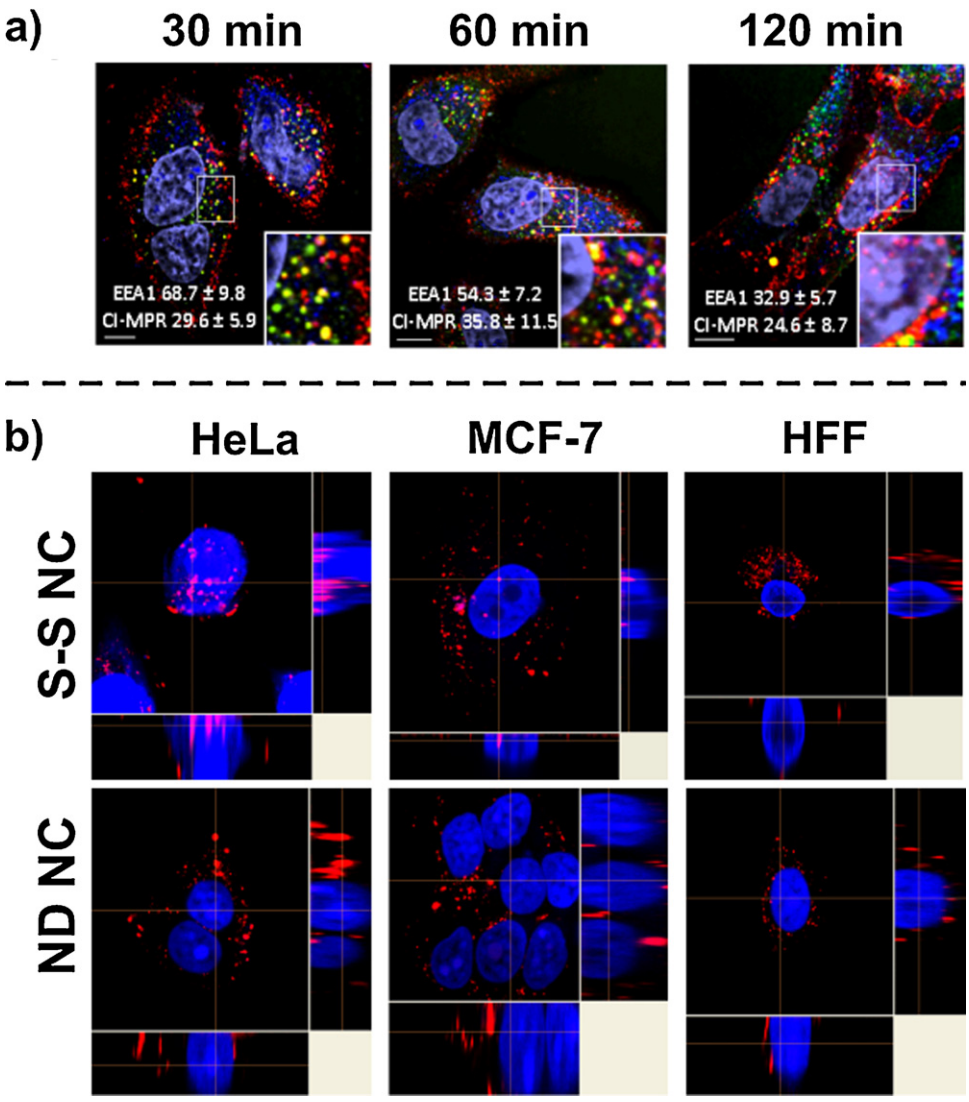

Figure 2 Protein nanocapsule cellular trafficking and localization. (a) The trafficking of Rho—APO in S—S NCs through endosomes. HeLa cells were incubated with 20 nM S—S Rho—APO NCs (red) at 37 °C for various time periods, 30, 60 and 120 min. Early endosomes were detected by early endosome antigen 1 (EEA1, green). Late endosomes were detected by cation-independent mannose-6-phosphate receptor (CI-MPR, blue). Nuclei were stained with DAPI and shown as purple. The scale bar represents 10 μm. The percentage of fluorescence colocalization was quantified by calculating colocalization coefficients using Manders' overlap coefficient (>10 samples) and shown in each figure; (b) confocal microscopy of cellular localization of Rho—APO encapsulated in S—S NC and ND NC to cancer cell lines HeLa and MCF-7, and noncancerous HFF. Nuclei were stained with DAPI (blue). The scale bar is 20 μm.

Tumor-selective cytotoxicity of apoptin nanocapsules

We then investigated whether the MBP—APO protein delivered still possesses its function to induce tumor-selective apoptosis. The potency and selectivity of S—S APO NC were tested on various cell lines including HeLa, MCF-7, MDA-MB-231, and HFF (Fig. 3a—d). MTS assay was used to measure cell viability 48 h after addition of the protein and NC. For each cell line, ND APO NC and native MBP—APO were used as negative controls. When S—S APO NC was added to a final concentration of 200 nM, all three cancer cell lines had no viable cells, whereas ~75% of the HFF had survived. The IC_{50} values were 80 and 30 nM for HeLa and MDA-MB-231, respectively. The IC_{50} for MCF-7 was higher at ~110 nM, which may be due to the deficiency in the terminal executioner caspase 3 and reliance on other effector caspases for apoptosis [29,30]. As expected, native MBP—APO and ND APO NC did not significantly decrease the viability of any cell lines tested, consistent with the inability to enter cells and release MBP—APO in cytoplasm, respectively. The IC_{50} values of S—S APO NC toward MDA-MB-231 increased as the surface charge of the NC became more neutral (Supplement 5), suggesting more efficient internalization can improve S—S NCs cytotoxicity. The morphologies of MDA-MB-231 and HFF cells were examined under various treatments. Only the S—S APO NC treated MDA-MB-231 cells exhibited blebbing and shrinkage, which are hallmarks of apoptotic cell death (Fig. 3e

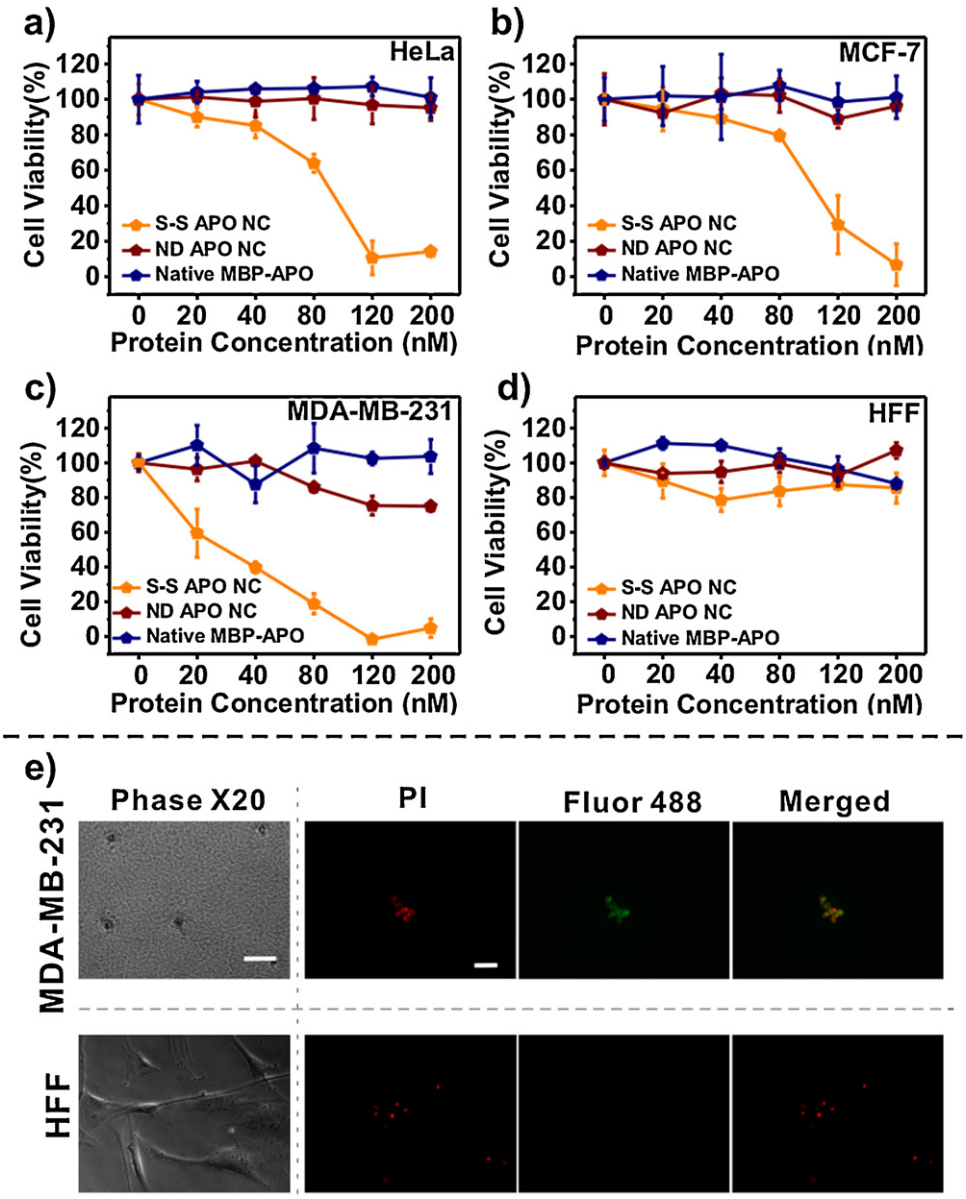

Figure 3 Cytotoxicity and apoptosis observed following nanocapsule delivery. (a) HeLa; (b) MCF-7; (c) MDA-MB-231; or (d) HFF cells with treatment of different concentrations of S—S APO NC, ND APO NC, and native MBP—APO. (e) Apoptosis induced by S—S APO NC determined by TUNEL assay. Images on the left are bright field microscopy images of MDA-MB-231 and HFF cells treated for 24 h with 200 nM S—S APO NC. The scale bar represents 50 μm. Images right of the dash line shows detection of apoptotic fragmentation of the nucleosome after same treatment using APO-BrdU™ TUNEL assay kit. The scale bar represents 50 μm. Red fluorescence represents the propidium-iodide (PI)-stained total DNA, and green fluorescence represents the Alexa Fluor 488-stained nick end label, the indicator of apoptotic DNA fragmentation. The merged pictures combine the PI-stained nuclei and the Alexa Fluor 488-stained nick end label. (Note the bright field images do not overlap with the fluorescent microscopy images; cells were detached and collected for TUNEL assay after treatment.)

and Supplement 7). Using TUNEL assay, S—S APO NC treated MDA-MB-231 also showed nuclear fragmentation associated with apoptosis, whereas cells treated with native MBP—APO and ND APO NC at the same concentration (Supplement 7), as well as HFF treated with 200 nM S—S APO NC (Fig. 3e), had no sign of apoptosis. Collectively, these results demonstrated that the recombinant MBP—APO delivered by the degradable NCs retains the potency and selectivity as the transgenically expressed apoptin in previous studies [9].

In vivo evaluation of apoptin nanocapsules

We further examined the potency of S—S APO NC in a mouse xenograft model. Female athymic nude (*nu*/*nu*) mice were subcutaneously grafted on the back flank with 5×10^6 MCF-7 breast cancer cells. When the tumor volume reached 100—200 mm^3 (day 0), mice were randomly separated into different groups and treated with intratumoral injection of PBS, MBP—APO, S—S APO NC. In addition, S—S NC with bovine serum albumin (S—S BSA NC) was added as a nonlethal

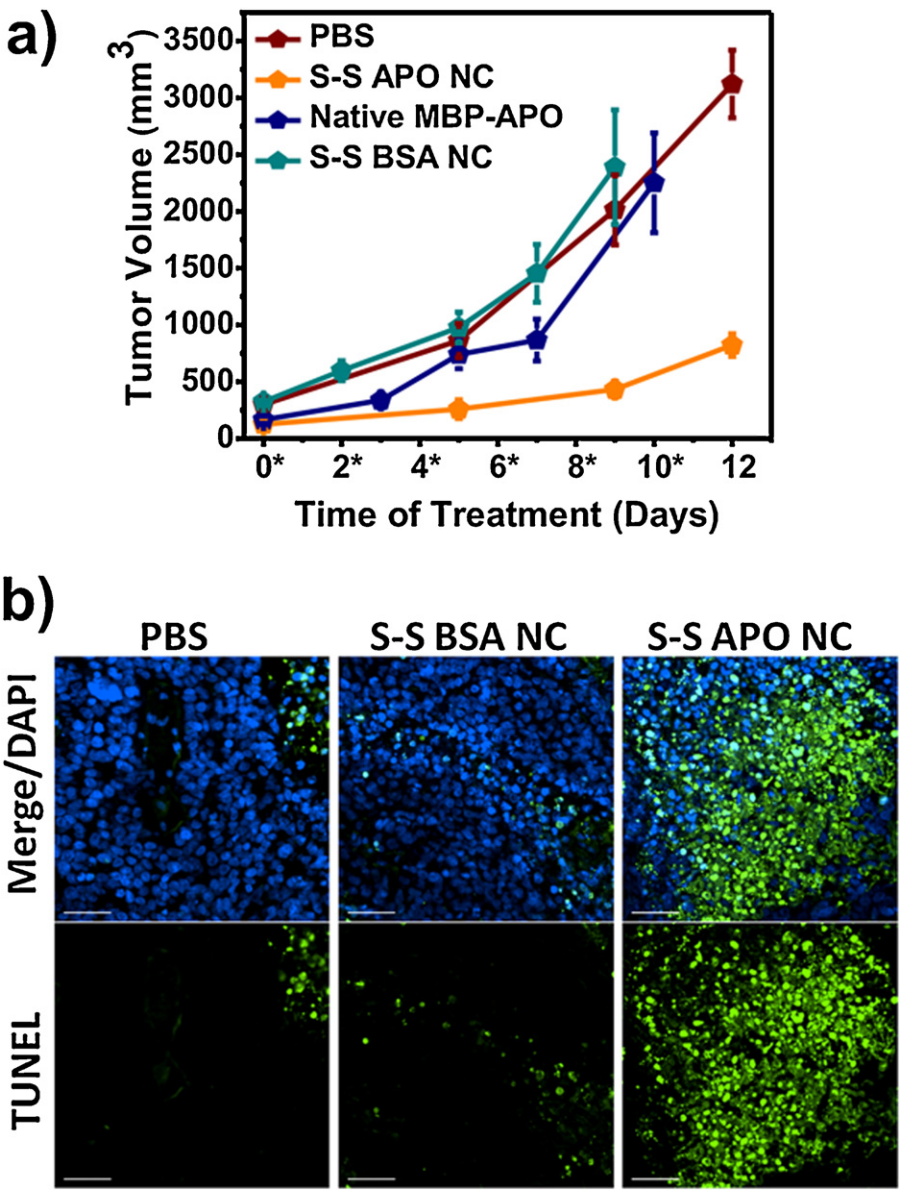

Figure 4 Treatment of apoptin nanocapsules resulted in tumor growth retardation. (a) Significant tumor inhibition was observed in the mice treated by S—S APO NC. Female athymic nude mice were subcutaneously grafted with MCF-7 cells and treated with intratumoral injection of MBP—APO ($n = 4$) or S—S APO NC ($n = 4$) (200 μg/mouse) every other day. PBS ($n = 3$) and S—S BSA NC ($n = 4$) were included as negative controls. The average tumor volumes were plotted *vs.* time. Asterisks indicate injection days. (b) Detection of apoptosis in tumor tissues after treatment with different NCs. Cross-sections of MCF-7 tumors were stained with fluorescein-dUTP (green) for apoptosis and DAPI for nucleus (blue). The scale bars represent 50 μm.

protein cargo control to test the effects of the S—S NC polymer component on tumor cells *in vivo*. Tumors treated with saline, S—S BSA NC or native MBP—APO expanded rapidly and reached the maximum limit (>2500 mm^3) within 12 days. In sharp contrast, tumor growth was significantly delayed when treated with S—S APO NC (Fig. 4a). Fixed tumor tissues collected from each treatment group were examined for DNA fragmentation using *in situ* TUNEL assay. The images revealed the highest level of cell apoptosis for the tumor harvested from mice treated with S—S APO NC, correlating well with the significantly delayed tumor growth observed for this treatment group and confirming that tumor growth inhibition was indeed due to apoptin-mediated apoptosis (Fig. 4b). Collectively, the xenograft study verified that the degradable NCs effectively delivered MBP—APO proteins to tumor cells *in vivo*, which was highly effective in limiting tumor progression. Upon further optimization of the pharmacokinetics of the S—S APO NC, including surface derivatization with active targeting ligands, these particles may be intravenously administered as an anticancer therapy [31].

Conclusions

We were able to deliver the high molecular weight complex of the tumor-selective MBP—APO using a redox-responsive polymeric NC *in vitro* and *in vivo*. The choice and design

of the sub-100 nm NC is well-suited for diverse protein targets because of its mild preparation conditions, reversible encapsulation, efficient membrane penetration, and cytoplasmic release of the protein cargo. Our application here further illustrates how intracellular protein delivery using nanoscale system can provide new possibilities for achieving selective anticancer therapy.

Acknowledgements

This work was supported by a David and Lucile Packard Foundation to Y.T.; a CDMRP BCRP Idea Award BC101380 to Y.T. and P.W. We thank Dr. C. Backendorf and Dr. M. Noteborn (Universiteit Leiden) for the expression plasmid of MBP—APO.

Appendix A. Supplementary data

Supplementary data associated with this article can be found, in the online version, at http://dx.doi.org/10.1016/j.nantod.2012.12.003.

References

[1] J.B. Gibbs, Science 287 (2000) 1969.
[2] J.H. Atkins, L.J. Gershell, Nat. Rev. Drug Discov. 1 (2002) 491.
[3] G.I. Evans, K.H. Vousden, Nature 411 (2001) 342.
[4] J.C. Reed, Cancer Cell 3 (2003) 17.
[5] T.G. Cotter, Nat. Rev. Cancer 9 (2009) 501.
[6] A. Russo, M. Terrasi, V. Agnese, D. Santini, V. Bazan, Ann. Oncol. 17 (2006) 115.
[7] C.J. Brown, S. Lain, C.S. Verma, A.R. Fersht, D.P. Lane, Nat. Rev. Cancer 9 (2009) 862.
[8] M.H.M. Noteborn, Eur. J. Pharmacol. 625 (2009) 165.
[9] C. Backendorf, A.E. Visser, A.G. de Boer, R. Zimmerman, M. Visser, P. Voskamp, Y.H. Zhang, M. Noteborn, Annu. Rev. Pharmacol. Toxicol. 48 (2008) 143.
[10] M. Los, S. Panigrahi, I. Rashedi, S. Mandal, J. Stetefeld, F. Essmann, K. Schulze-Osthoff, Biochim. Biophys. Acta 1793 (2009) 1335.
[11] S.M. Zhuang, A. Shvarts, H. van Ormondt, A.G. Jochemsen, A.J. van der Eb, M.H. Noteborn, Cancer Res. 55 (1995) 486.
[12] J.G. Teodoro, D.W. Heilman, A.E. Parker, M.R. Green, Genes Dev. 18 (2004) 1952.
[13] A.A.A.M. Danen-Van Oorschot, D.F. Fischer, J.M. Grimbergen, B. Klein, S.M. Zhuang, J.H.F. Falkenburg, C. Backendorf, P.H.A. Quax, A.J. Van der Eb, M.H.M. Noteborn, Proc. Natl. Acad. Sci. U.S.A. 94 (1997) 5843.
[14] S.R. Leliveld, Y.H. Zhang, J.L. Rohn, M.H. Noteborn, J.P. Abrahams, J. Biol. Chem. 278 (2003) 9042.
[15] A.A.A.M. Danen-Van Oorschot, Y.H. Zhang, S.R. Leviveld, J.L. Rohn, M.C.M.J. Seelen, M.W. Bolk, A. van Zon, S.J. Erkeland, J.P. Abrahams, D. Mumberg, M.H.M. Noteborn, J. Biol. Chem. 278 (2003) 27729.
[16] J.L. Rohn, Y.H. Zhang, R.I. Aalbers, N. Otto, J. Den Hertog, N.V. Henriquez, C.J. Van De Velde, P.J. Kuppen, D. Mumberg, P. Donner, M.H. Noteborn, J. Biol. Chem. 277 (2002) 50820.
[17] A.M. Pietersen, M.M. van der Eb, H.J. Rademaker, D.J. van den Wollenberg, M.J. Rabelink, P.J. Kuppen, J.H. van Dierendonck, H. van Ormondt, D. Masman, C.J. van de Velde, A.J. van der Eb, R.C. Hoeben, M.H. Noteborn, Gene Ther. 6 (1999) 882.
[18] M.M. van der Eb, A.M. Pietersen, F.M. Speetjens, P.J. Kuppen, C.J. van de Velde, M.H. Noteborn, R.C. Hoeben, Cancer Gene Ther. 9 (2002) 53.
[19] D.J. Peng, J. Sun, Y.Z. Wang, J. Tian, Y.H. Zhang, M.H. Noteborn, S. Qu, Cancer Gene Ther. 14 (2007) 66.
[20] M.L. Edelstein, M.R. Abedi, J. Wixon, J. Gene Med. 9 (2007) 833.
[21] L. Guelen, H. Paterson, J. Gaken, M. Meyes, F. Farzaneh, M. Tavassoli, Oncogene 23 (2004) 1153.
[22] J. Sun, Y. Yan, X.T. Wang, X.W. Liu, D.J. Peng, M. Wang, J. Tian, Y.Q. Zong, Y.H. Zhang, M.H.M. Noteborn, S. Du, Int. J. Cancer 124 (2009) 2973.
[23] C. Murriel, S. Dowdy, Expert Opin. Drug Deliv. 3 (2006) 739.
[24] J. Shi, A.R. Votruba, O.C. Farokhzad, R. Langer, Nano Lett. 10 (2010) 3223.
[25] Z. Gu, A. Biswas, M. Zhao, Y. Tang, Chem. Soc. Rev. 40 (2011) 3638.
[26] P.P. Adiseshaiah, J.B. Hall, S.E. McNeil, Nanomed. Nanobiotechnol. 2 (2010) 99.
[27] Z. Gu, M. Yan, B. Hu, K.I. Joo, A. Biswas, Y. Huang, Y. Lu, P. Wang, Y. Tang, Nano Lett. 9 (2009) 4533.
[28] M. Zhao, A. Biswas, B.L. Hu, K.I. Joo, P. Wang, Z. Gu, Y. Tang, Biomaterials 32 (2011) 5223.
[29] M. Burek, S. Maddika, C.J. Burek, P.T. Daniel, K. Schulze-Osthoff, M. Los, Oncogene 25 (2006) 2213.
[30] R.U. Janicke, M.L. Sprengart, M.R. Wati, A.G. Porter, J. Biol. Chem. 273 (1998) 9357.
[31] N. Kamaly, Z. Xiao, P.M. Valencia, A.F. Radovic-Moreno, O.C. Farokhzad, Chem. Soc. Rev. 41 (2012) 2971.

Muxun Zhao obtained her B.S. degree in Biochemistry, Biology and Biotechnology from Worcester Polytechnic Institute in 2009. She then joined the Department of Chemical and Biomolecular Engineering at University of California, Los Angeles for graduate studies. She is now a fourth year Ph.D. student in Professor Yi Tang's laboratory. Her current research interests include bionanotechnology and biomaterials towards cancer treatment.

Biliang Hu received his B.S. in Biology at University of Science and Technology of China in 2007. He is currently a Ph.D. student in Department of Chemical Engineering and Materials Science at University of Southern California. He has worked on various research topics, ranging from dendritic cell-directed lentiviral vectors for cancer vaccines, biodegradable polymer matrix for immune modulation, nanoparticles for protein delivery, peptide design towards high stability and efficient oral availability, and antibody-directed modulation of tumor microenvironment.

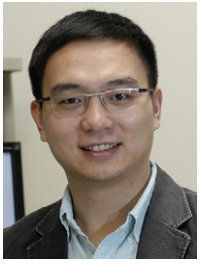

Dr. Zhen Gu obtained his Ph.D. degree in 2010, with a major in MEMS and nanotechnology at University of California, Los Angeles, under the guidance of Prof. Yi Tang in the Department of Chemical and Biomolecular Engineering. He was a postdoctoral associate working with Prof. Robert Langer at Massachusetts Institute of Technology and Harvard Medical School during 2010 to 2012. He is currently an assistant professor in the joint Department of Biomedical Engineering at University of North Carolina at Chapel Hill and North Carolina State University. He also holds an adjunct position in the UNC Eshelman School of Pharmacy. His research interests include controlled drug delivery, bio-inspired materials, implantable devices and biochip technology.

Dr. Kye-Il Joo, Ph.D., is currently a postdoctoral research associate at Department of Chemical Engineering and Materials Science, University of Southern California. He obtained his B.S. from Hanyang University, Korea (2002) and Ph.D. from Viterbi School of Engineering, University of Southern California (2009). He has a broad training in biochemical engineering, nanotechnology, biomaterials, and immunobioengineering. His recent research is focused on the design of crosslinked multilamellar liposomal nanoparticles for controlled release of anticancer drugs, as well as the design of biodegradable hydrogels to modulate immune cells for enhanced vaccination.

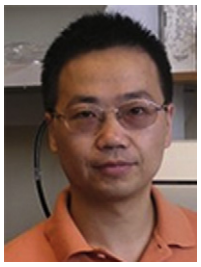

Dr. Pin Wang is an associate professor in the Department of Chemical Engineering and Materials Science, Department of Biomedical Engineering, and Department of Pharmacology and Pharmaceutical Science at University of Southern California (USC). He received his Ph.D. in 2003 from California Institute of Technology (Caltech). After a postdoctoral study at Caltech, he joined USC as an assistant professor in 2005. Dr. Wang's research focuses on engineering viral vectors for targeted gene delivery, dendritic cell-directed vaccines against cancers and infectious disease, tumor microenvironment, and design of nanoparticles for drug delivery.

Dr. Yi Tang obtained his B.S. degrees in Chemical Engineering and Material Science from Penn State University in 1997. He then moved to California Institute of Technology and studied biopolymer biosynthesis under the guidance of Prof. David A. Tirrell. After obtaining his Ph.D. in 2002, he moved to Stanford University to study biosynthesis with Prof. Chaitan Khosla. In 2004, he began his independent academic career in the Department of Chemical and Biomolecular Engineering at the University of California, Los Angeles, where he is now the Chancellor's Professor. He currently holds a joint appointment in the Department of Chemistry and Biochemistry. His group studies bionanotechnology, natural product biosynthesis and biocatalysts.